Three-year observations of ozone columns over polar vortex edge area above West Antarctica

Yuanyuan Qian[1,2], Yuhan Luo*[1], Fuqi Si[1], Taiping Yang[1], and Dongshang Yang[1]

[1]*Key Laboratory of Environmental Optical and Technology, Anhui Institute of Optics and Fine Mechanics, Hefei Institutes of Physical Science, Chinese Academy of Sciences, Hefei 230031, China*

[2]*University of Science and Technology of China, Hefei 230026, China*

ABSTRACT

The ozone vertical column densities (VCDs) were retrieved by Zenith Scattered Light-Differential Optical Absorption Spectroscopy (ZSL-DOAS) from January 2017 to February 2020 over Fildes Peninsula, West Antarctica (62.22S, 58.96W). The retrieved ozone VCDs started to decline around July with a comparable gradient (around 1.4 DU/day), then dropped to the lowest level in September and October, when the ozone holes appeared (less than 220 DU). The daily mean values of ozone columns were compared with OMI and GOME-2 satellite observations and MERRA-2 reanalysis dataset, with the correlation coefficients (R^2) of 0.86, 0.94 and 0.90 respectively. To better understand the causes of ozone depletion, the retrieved ozone columns, temperature and potential vorticity (PV) at certain altitude were analyzed. The profiles of ozone and PV showed positive correlation during the fluctuations, which indicates that polar vortex has great influence on stratospheric

*Corresponding author: Yuhan Luo
Email: yhluo@aiofm.ac.cn

ozone depletion during Antarctic spring. Located at the edge of polar vortex, the observed data will provide a basis for further analysis and prediction of the inter-annual variation of stratospheric ozone in future.

Key words: ozone VCDs, ZSL-DOAS, Antarctic ozone depletion, polar vortex

Citation: Qian, Y. Y., Y. H. Luo, F. Q. Si, T. P. Yang, and D. S. Yang, 2021: Three-year observations of ozone columns over polar vortex edge area above West Antarctica. *Adv. Atmos. Sci.*, https://doi.org/10.1007/s00376-021-0243-7.

Article Highlights:

- The ozone VCDs retrieved by ZSL-DOAS from ground-based data validate the satellite observations in Fildes Peninsula.
- The retrieved ozone VCDs indicated that ozone holes appeared over the Fildes Peninsula, West Antarctica, with sharp fluctuations during spring.
- Polar vortex has great influence on stratospheric ozone depletion during Antarctic spring.

1. Introduction

Ozone is an important trace gas in the earth's atmosphere, which plays a key role in the environment, climate change and human health (Li et al., 2015). It is mainly distributed about 20-35 km away from the surface of the earth, which can absorb UV radiation to protect life on Earth. The ozone hole was firstly found by Farman in Argentine Islands (65°S, 64°W) and Halley Bay (76°S, 27°W), Antarctica (Farman et al., 1985). The long-term ozone column measurements, obtained from South Pole station and SBUV satellite observations, indicated that the healing of Antarctic ozone holes is emerging with the control of Hydrochlorofluorocarbons emissions (Solomon et al., 2016).

The ozone columns over Antarctica are mainly obtained from satellite observations, ground-based DOAS observations, Brewer spectrophotometers, and Dobson spectrophotometers (Čížková et al., 2019; Kokhanovsky et al., 2020). Satellite observations and ECMWF data were analyzed to study the influence of stratospheric halogen species (mainly Cl and Br) in polar vortex which may lead to the ozone depletion over Antarctica (Marsing et al., 2019; Nakajima et al., 2020). The quality of satellite ozone observations was affected by polar vortex (Paschou et al., 2020). In addition, atmospheric and chemical transport model is also used for the analysis of long-term ozone trends and troposphere-stratosphere exchange in Antarctica (Hegglin and Shepherd, 2009; Lu et al., 2019). The accurate retrieval of ozone columns, accompanied with the analysis of stratospheric chemistry, dynamic and temperature changes are necessary for the analysis of Antarctic ozone changes.

The atmosphere over Antarctica is controlled by strong polar vortex in winter, making it difficult to exchange with mid-latitude atmosphere. The extremely low air temperatures (<195K) inside the polar vortex, lead to the formation of polar stratospheric clouds (PSCs). PSCs, composed of nitrate trihydrate, water ice, etc, provide the surfaces for heterogeneous reactions that convert halogen reservoirs to active halogens with severe ozone depletion (~~FRIEβ~~Frieβ et al., 2005; Drdla ~~et~~ and Müller~~al.~~, 2012; Marsing et al., 2019). There are three types of PSCs decided by their state, including nitric acid trihydrate (NAT), supercooled ternary solution (STS) and ice PSCs, and corresponding to the temperatures of T_{nat} (195 K), T_{sts}, T_{ice}. Our observation site is located at the edge of the polar vortex, which is different from other inland stations (high latitudes) where the ozone columns continued to be low in spring. The rapid changes and great fluctuations of total ozone can be detected here, which are sensitive to the dynamic and chemical changes of PSCs.

As a kind of spectroscopic technique, differential optical absorption spectroscopy (DOAS) has been proved to be powerful, which has been widely used to monitor a variety of atmospheric trace gases (Stutz and Platt, 1997; Meller and Moortgat, 2000; Platt and Stutz, 2008). Zenith Scattered Light-DOAS (ZSL-DOAS) is suitable for measuring stratospheric gases, such as stratospheric NO_2, O_3 (Pommereau, 1982; Perner et al., 1994). Since the 1970s, numerous spaceborne UV detection instruments (such as OMI, GOME-2, MLS) have entered orbit to obtain the information of global trace gases, which provided comprehensive information of ozone holes and changes (Sonkaew et al., 2013; Zhang et al., 2015; Kuttippurath and Nair, 2017). The advantages of ZSL-DOAS are that it has low energy consumption and can be unattended, and it is less affected by changes of meteorological conditions in boundary layer, temperature and clouds.

In this paper, daily variations of ozone vertical column densities (VCDs) were retrieved by ZSL-DOAS, and taken a correlation analysis with the observations of Ozone Monitoring Instrument (OMI) and Global Ozone Monitoring Experiment 2 (GOME-2). Combining the low-stratospheric PV profiles, we analyzed the cause of ozone depletion leading to ozone holes from September to October in 2017 and 2018 in this region. The novelty of this study is to analyze the correlation between ozone depletion and PV at the edge of polar vortex, where ozone depletion is more sensitive to the change of PV.

2. Experiments and data analysis

2.1 *Experiments site*

The experiment site and DOAS instrument are shown in Figure 1. The red star is the location of Chinese Great Wall Station (62.22S, 58.96W) in Fildes Peninsula, South Shetland Islands. The red region is the area of the OMI pixel, and the yellow region is the area of the GOME-2 pixel.

Ground-based passive DOAS system used in this experiment is composed of a prism, telescope, motor, filter, CCD spectrometer, computer and so on. The wavelength range of the spectrometer is 290-420 nm, with the spectral resolution of 0.3 nm. In this experiment, the data from zenith direction was used to retrieve the slant column densities (SCDs) of ozone.

2.2 *Principle of the DOAS method*

The DOAS method retrieves concentration of trace gases by its characteristic absorption and measured intensity, which is based on Lambert-Beer's law. From

Lambert-Beer's law and derivation:

$$\ln\frac{I^*(\lambda)}{I_0(\lambda)}=\sum\left(\sigma_j^*(\lambda)\cdot c_j\cdot L\right)=\sum\left(\sigma_j^*(\lambda)\cdot SCD_j\right) \quad (1)$$

Here, $I_0(\lambda)$ denotes the original luminous intensity of the radiator, $I^*(\lambda)$ represents the measured intensity after filtering through a gas layer of length L, $\sigma_j^*(\lambda)$ denotes the broadband absorption cross section at the wavelength λ, c_j represents the average concentration of gas j. $SCD_j=\int c_j\cdot L$, called slant column density of j. $D=\ln\frac{I^*(\lambda)}{I_0(\lambda)}$, named differential optical density. The SCD of desired trace gas can be retrieved through least-squares fitting by Eq. (1).

2.3 *spectral retrieval*

The ozone SCDs were retrieved from the QDOAS software developed by the Royal Berlin Institute for Space Aeronomy (BIRA-IASB) (http://uv-vis.aeronomie.be/software/QDOAS/), with a retrieval wavelength range of 320-340 nm. O_3, NO_2, O_4 and ring calculated by Ring.exe of QDOAS cross sections are considered in the retrieval algorithm, detailed parameters are shown in Table 1. The daily noon zenith spectrum was used as the reference spectrum for SCD retrieval. Taking the fits of spectrum from February 24, 2018 as an example (Figure 2), the ozone dSCD is 5.20×10^{18} molec/cm^2, with the fitting residual of 9.76×10^{-4}.

2.4 *Calculation of ozone VCDs*

The ZSL-DOAS method is powerful in measuring stratospheric gases such as ozone, because 90% of which is distributed in the stratosphere. To convert SCD which is related to the viewing angles into vertical column density (VCD), we need to introduce the Air Mass Factor (AMF). The relationship between SCD and VCD is as follows:

$$AMF = \frac{SCD}{VCD} \quad (2)$$

AMFs were retrieved by atmospheric radiative transfer model SCIATRAN. The a-priori profiles of ozone, temperature and pressure used to obtain AMFs are the monthly average profiles of SCIATRAN profiles database, which are selected by month and latitude. The Fraunhofer absorption which will have a great influence on the retrieval of gas concentration should be removed (Platt and Stutz, 2008). The slant column concentration after deducting Fraunhofer absorption is expressed by the differential slant column concentration (dSCD):

$$dSCD(\alpha,\beta) = SCD(\alpha,\beta) - SCD_{FRS} = AMF(\alpha,\beta)\cdot VCD - SCD_{FRS} \quad (3)$$

Here, SCD_{FRS} means Fraunhofer absorption part. The above formula is in y=ax+b format, so we can use AMF as the abscissa and dSCD as the ordinate to perform linear fitting, the slope is VCD, and the absolute value of the intercept is the Fraunhofer absorption part. Taking the retrieved data in February 24, 2018 as an example, the linear fit of ozone dSCDs and AMFs on that day is shown in Figure 3. The calculated ozone VCD is 7.322×10^{18} $\mathrm{molec/cm^2}$, the error is 2.232×10^{16} $\mathrm{molec/cm^2}$. The ozone VCD was calculated by the average of VCD_{am} (the VCD of morning) and VCD_{pm} (the VCD of afternoon).

The uncertainty of ozone VCD retrieval through ZSL-DOAS method comes from the retrieval of SCD and AMF. The comprehensive estimation of uncertainty of ozone

SCDs is 1.475 % (95 % confidence interval, N=76902). We considered the parameters including SZA (solar zenith angle), surface albedo, a-priori ozone profile and wavelength, which would influence the values of AMF. In this study, SZA used for calculation is between 35° and 80°, and the surface albedo is between 0.08 and 0.6. The a-priori profile of ozone is obtained from the monthly mean climatology. **The detailed parameter nodes to estimate the uncertainty of AMF on wavelength are shown in Table 2. The AMF uncertainty caused by wavelength selection was calculated through $(AMF_{\lambda} - AMF_{328})/AMF_{\lambda}$, λ denotes wavelength. In the simulated parameter nodes (Table 2), the AMF uncertainty on wavelength is between -4.257 % and 4.630 %, with the averaged absolute uncertainty of 2.030 %. According to the analysis of OMI ozone product, the variations of AMF influenced by a-priori profiles of ozone are small (2 % on the 95 % confidence interval) (Bhartia, 2002). Therefore, the averaged AMF uncertainty with this method is calculated through $\sqrt{AMF_{uncertainty\_wave}^2 + AMF_{profile}^2}$, namely 2.85 %.** The total uncertainty of VCD is 3.21 % through error propagation formula as follows:

$$VCD_{uncertainty} = \sqrt{\left(SCD_{uncertainty}^2 + AMF_{uncertainty}^2\right)} \qquad (4)$$

2.5 *Auxiliary data*

The daily ozone VCDs observed by OMI and GOME-2 from January 2017 to February 2020 were obtained in this study. The OMI instrument, launched on July 15, 2004, is onboard the Aura satellite, which is a nadir scanning instrument (Xie et al., 2016). The field of view of OMI can reach 114°, which permits the daily global coverage. The OMI instrument can measure ozone in UV (270-380 nm) and VIS (350-500 nm) wavelengths. The spectral resolution of OMI is 0.5 nm, with high spatial resolution of $13 \times 24\,\mathrm{km}^2$ (Thomas et al., 2011). The daily ozone VCDs of OMI (https://disc.gsfc.nasa.gov/) were used to compare with ZSL-DOAS observations.

GOME-2 is a UV/VIS nadir observation spectrometer, which is onboard the MetOp-A satellite and was launched on October 19, 2006 by European Space Agency (ESA). The ozone data sets of GOME-2 are retrieved by the GODFITv.4 algorithm. The wavelength range of GOME-2 instrument is 240-790 nm. The spectral resolution of GOME-2 is 0.2-0.5 nm, with spatial resolution of $80 \times 40\,\mathrm{km}^2$ (Koukouli et al., 2014). The ozone VCDs obtained from GOME-2 data set (https://avdc.gsfc.nasa.gov/) are daily mean VCDs of the overpass data.

The temperature and ozone profiles used here were obtained from Modern-Era Retrospective analysis for Research and Applications version 2 (MERRA-2) data, which are available every 3 hours. The MERRA-2 is an atmospheric reanalysis database, obtained from Goddard Earth Observing System Model, version 5 (GEOS-5) with Atmospheric Data Assimilation System (ADAS) (Ganeshan and Yang, 2019). The spatial resolution of MERRA-2 is $0.5^{\circ} \times 0.625^{\circ}\,(\mathrm{lat} \times \mathrm{lon})$ with 72 model levels. The data of ozone profiles and temperature at 50 hPa from MERRA-2 data sets (https://disc.gsfc.nasa.gov/) are the averaged data of the whole day.

The daily PV data used in this paper is obtained from ERA Interim datasets of

European Centre for Medium-Range Weather Forecasts (ECMWF) (https://www.ecmwf.int/). ERA Interim is a reanalysis data with six hours' interval, which is available from January 1985 to August 2019. The ERA Interim data sets were obtained from the data assimilation system of Integrated Forecast System (IFS), released in 2006. The spatial resolution of ERA Interim data is $0.25^{\circ} \times 0.25^{\circ}$ (lat $\times$ lon), with 60 levels in the vertical direction from the surface to 0.1 hPa. In this paper, the daily PV data set at 12:00 from 2017 to 2018 was used to analyze the ozone depletion.

3. Results and discussion

3.1 *Meteorological conditions*

The meteorological conditions of the Fildes Peninsula are shown in Figure 4 and Figure 5, which represent temperatures (at 50 hPa) and PV (on isentropic level of 475 K) respectively. T_{nat} denotes the threshold temperature for the formation of PSCs. The temperature trends showed that the formation of PSCs began around June, which is corresponding to the development of polar vortex in early winter (Frieß ~~Frieβ~~ et al., 2005). The overall temperature of 2019 is higher than that of 2018 and 2017 and has an early termination, which leads to the short existence of PSCs.

Potential vorticity (PV) is used to represent the capacity for air mass to rotate in the atmosphere and define the edge of polar vortex, calculated by temperature, wind field information and so on. The units of PV are divided into SI units ($\mathrm{K\,m^2 kg^{-1} s^{-1}}$) and potential vorticity units (PVU), $1\ \mathrm{PVU} = 10^{-6}\ \mathrm{K\,m^2 kg^{-1} s^{-1}}$. In Figure 5, we take the 475 K potential temperature surface which corresponds to the low stratosphere as the criterion to define the edge of polar vortex (Paschou et al., 2020), where blue lines denote the PV of the Fildes Peninsula and red lines denote the PV of vortex edge. Here we used the Nash's criterion to determine the edge of the polar vortex, where the gradient of PV is the highest of the southern hemisphere along the equivalent latitude (Nash et al., 1996). The blue line below and above the red line indicate that the Fildes Peninsula was located inside and outside of the polar vortex, respectively. The number of days inside and outside the polar vortex boundary in 2017 and 2018 is shown in Table 3.

3.2 *Results of ozone VCDs*

Satellite ozone observations may have large biases at high latitudes, especially when the SZAs are large. Therefore, the SZAs used to obtain ozone VCDs from satellite observations are less than 86°. The ZSL-DOAS observations in this research can be used to validate the satellite observations at high latitude.

The ozone VCDs retrieved from ZSL-DOAS instrument, MERRA-2 dataset and that from OMI and GOME-2 satellite observations from January 2017 to February 2020 are shown in Figure 6 (a), where black line located at 220 DU ($1\ \mathrm{DU} = 2.69 \times 10^{16}\ \mathrm{molec/cm^2}$) denotes the threshold for ozone hole (Bodeker et al., 2002). The biases between OMI, GOME-2, MERRA-2 and ZSL-DOAS are shown in Figure 6 (b). The standard deviations between GOME-2, MERRA-2 and ZSL-DOAS are shown in Figure 6 (c). OMI and GOME-2 are nadir observations that are different from the zenith observation method of ZSL-DOAS. The ozone VCDs of satellite observations were obtained at overpass time (13:30 LT and 9:30 LT), which may lead to the large biases and standard deviations when ozone fluctuated greatly at that day.

The averaged ozone VCDs and days of ozone holes for 2017, 2018 and 2019 over the Fildes Peninsula are shown in Table 4. The ozone VCDs started to decline around July with a comparable gradient (around 1.4 DU/day), which is in agreement with the formation of PSCs in Antarctic winter. The ozone VCDs declined further in the spring, with severe ozone depletion in September and October, and then gradually returned to normal levels. During the severe ozone depletion periods in September and October, which leads to the ozone holes (<220 DU), we discussed the correlation between polar vortex and ozone concentration in detail in section 3.3. The linear fits of the retrieved ozone VCDs with OMI and GOME-2 satellite observations and MERRA-2 dataset are shown in Figure 7. The correlation coefficients (R^2) are 0.86, 0.94 and 0.90 respectively.

3.3 *Influence of PV on ozone depletion*

The value of PV is negative in Antarctica while positive in Arctic. Closely related to the polar vortex, the absolute value of PV is generally greater inside polar vortex. The PSCs formed inside the polar vortex can activate the halogen species, which lead to severe ozone depletion. The PV, temperatures (at 50 hPa) and retrieved ozone VCDs from September to October during the observation periods are shown in Figure 8. As shown in Figure 8 (a) (b) (c) (d), the trend of PV and ozone VCDs is at the same pace, in other words, PV is positively correlated with the ozone VCDs. The ozone VCDs fluctuated between 170-405 DU from September to October of 2017. The fluctuations in 2018 was between 150-290 DU. The relationship between PV and ozone VCDs was more obvious in 2017 with greater fluctuations. As shown in Figure 8 (a), ozone recovered to its peaks at 22 September, 9 October, 19 October and 28 October 2017, when Fildes Peninsula was all out of the polar vortex. The retrieved ozone VCDs fluctuated with the same pattern as the temperatures at 50 hPa, which means ozone was depleted inside the polar vortex, where the temperature is lower. Therefore, polar vortex has great influence on stratospheric ozone depletion during Antarctic spring.

Ozone and PV profiles above the Fildes Peninsula during spring of 2017 and 2018 were analyzed as well. The averaged ozone profiles during the ozone hole periods and non-ozone hole periods from September to October in 2017 were demonstrated (Figure 9). The averaged ozone profiles and the percentage of ozone loss at different heights indicated that the maximum ozone loss was about 63% at the height of 19.5 km. PV might differ more than ten times with different heights in low stratosphere, which indicated that a small and sensitive height layer should be chosen to discuss its influence on ozone depletion. Therefore, we chose the profiles height at 19-20 km, where the photochemical reactions destroying ozone were most severe.

Since the observation site is located near the edge of polar vortex, it is sensitive to the change of polar vortex. The synchronized change between ozone and PV indicated the critical influence of polar vortex on ozone depletion. The profiles of ozone and PV at the height of 19-20 km from September to October in 2017 and 2018 were shown in Figure 10. The ozone concentration at the height of 19-20 km fluctuated between

0.65-6.87 ppmv and 0.54-7.30 ppmv in 2017 and 2018, respectively. The absolute value of PV showed obvious increase when the ozone concentration was decreased. The ozone depletion in Antarctic spring, which leads to the formation of ozone holes, is closely related to PV. Located at the edge of polar vortex, the observed data will provide a basis for further analysis and prediction of the inter-annual variation of stratospheric ozone in future.

4. Conclusion

In this paper, the daily ozone VCDs were retrieved by ZSL-DOAS from ground-based observation of DOAS instrument, and then linearly fitted with that from OMI and GOME-2 satellite observations and MERRA2 reanalysis dataset. Their correlation coefficients (R^2) are 0.86, 0.94 and 0.90 respectively, which validate the satellite observations and MERRA-2 dataset at this area.

In the spring of observation periods, the occurrences of ozone holes over the Fildes Peninsula were detected, when the daily ozone VCDs fluctuated sharply. Especially in September 2017, the daily fluctuations of ozone VCDs can reach 100 DU. The ozone VCDs began to decline in early winter with a comparable gradient (1.4 DU/day) during the observation periods, with the formation of PSCs. The ozone concentration began to recover at the end of October, and returned to the normal levels after November.

In this paper, PV was used as an indicator for analysis, which was positively correlated with ozone concentration over Fildes Peninsula in spring. The polar vortex of Antarctic spring has great influence on stratospheric ozone depletion.

It should be noted that the uncertainty estimation of AMF calculation is preliminary, and the uncertainty caused by the a-priori ozone profiles needs further analysis. More accurate a-priori ozone profiles (like column-dependent total ozone profiles) and the better reference spectrum (from direct-sun data) will be done in future research.

The observations of ozone VCDs over Fildes Peninsula will be continually conducted to observe the long-term ozone trends in this region. The observations conducted in this study are also valuable for validating modelled ozone concentrations in this region, and contribute to better understanding of ozone recovery and stratosphere-troposphere exchange over polar vortex edge area.

Acknowledgements. This research was financially supported by the National Natural Science Foundation of China (Grant Nos. 41676184 and 41941011). The authors gratefully acknowledge ECMWF (https://www.ecmwf.int/) for providing ERA-Interim reanalysis data and GES-DISC (https://disc.gsfc.nasa.gov/) for providing MERRA-2 data. The authors thank the staff of Great Wall station for their kind help. The authors acknowledge three anonymous referees for their help on the improvement of the manuscript.

REFERENCES

Bhartia, P. K., 2002: "OMI Algorithm Theoretical Basis Document: Volume Ⅱ, OMI Ozone Products", ATBD-OMI-02, August. [Available from https://docserver.gesdisc.eosdis.nasa.gov/repository/Mission/OMI/3.3_ScienceDataProductDocumentation/3.3.4_ProductGenerationAlgorithm/ATBD-OMI-02.pdf]

Bodeker, G. E., H. Struthers, and B. J. Connor, 2002: Dynamical containment of Antarctic ozone depletion. *Geophys. Res. Lett.*, **29**(7), ~~2-1-2-4~~1098, https://doi.org/10.1029/2001GL014206.

Bogumil, K., ~~J. Orphal, T. Homann, S. Voigt, P. Spietz, O. C. Fleischmann, A. Vogel, M. Hartmann, H. Kromming, H. Bovensman, J. Frerick,~~ and Coauthors~~J. P. Burrows~~, 2003: Measurements of molecular absorption spectra with the SCIAMACHY pre-flight model: Instrument characterization and reference data for atmospheric remote-sensing in the 230–2380 nm region. *Journal of Photochemistry and Photobiology A: Chemistry*, **157**(2--3): 167--~~–~~184, https://doi.org/10.1016/S1010-6030(03)00062-5.

Čížková, K., K. Láska, L. Metelka, and M. Staněk, 2019: Intercomparison of ground- and satellite-based total ozone data products at Marambio base, Antarctic Peninsula region. *Atmosphere*, **10**(11), 721, https://doi.org/10.3390/atmos10110721.

Drdla, K., and R. Müller, 2012: Temperature thresholds for chlorine activation and ozone loss in the polar stratosphere. *Annales Geophysicae*~~*Ann. Geophys.*~~, **30**(~~264~~7), 1055--1073, https://doi.org/10.5194/angeo-30-1055-2012.

Farman, J. C., B. G. Gardiner, and J. D. Shanklin, 1985: Large losses of total ozone in Antarctica reveal seasonal ClO_x/NO_x ~~ClO_x/NO_x~~ interaction. *Nature*, **315**, 207--210, https://doi.org/10.1038/315207a0.

Frieβ, U., K. Kreher, P. V. Johnston, and U. Platt, 2005: Ground-based DOAS measurements of stratospheric trace gases at two Antarctic stations during the 2002 ozone hole period. *J~~ournal~~. ~~of the~~ Atmos~~pheric~~. Sci~~ences~~.*, **62**(3), 765--777, https://doi.org/10.1175/JAS-3319.1.

Ganeshan, M., and Y. K. Yang, 2019: Evaluation of the Antarctic boundary layer thermodynamic structure in MERRA2 using dropsonde observations from the concordiasi campaign. *Earth and Space Science*, **6**, 2397--2409, https://doi.org/10.1029/2019EA000890.

Hegglin, M. I., and T. G. Shepherd, 2009: Large climate-induced changes in ultraviolet index and stratosphere-to-troposphere ozone flux. *Nature Geoscience*, **2**, 687--691, https://doi.org/10.1038/ngeo604.

Hermans, C., A. C. Vandaele, S. Fally, M. Carleer, R. Colin, B. Coquart, A. Jenouvrier, and M. F. Merienne, 2003: Absorption cross-section of the collision-induced bands of oxygen from the UV to the NIR.~~—~~ *Weakly Interacting Molecular Pairs: Unconventional Absorbers of Radiation in the Atmosphere*~~*Earth and Environmental Sciences*~~, C. Camy-Peyret and A. A. Vigasin, Eds., Springer~~27~~, 193--202, https://doi.org/10.1007/978-94-010-0025-3_16.

Kokhanovsky, A. A., M. Lamare, and V. Rozanov, 2020: Retrieval of the total ozone over Antarctica using Sentinel-3 ocean and land colour instrument. *Journal of Quantitative Spectroscopy and Radiative Transfer*, **251**, 107045, https://doi.org/10.1016/j.jqsrt.2020.107045.

Koukouli, M. E., ~~L. Clarisse, E. Carboni, Gent. J. V, C. Spinetti, D. Balis, S. Dimopoulos, R. Grainger,~~ and Coauthors~~N. Theys~~, 2014: Intercomparison of Metop-A SO_2 measure- ments during the 2010- 2011 Icelandic eruptions. *Annals of Geophysics*, **57**~~(2)~~, 2110, https://doi.org/10.4401/ag-6613.

Kuttippurath, J., and P. J. Nair, 2017: The signs of Antarctic ozone hole recovery. *Scientific Reports*~~*Sci. Rep.*~~, **7**, 585, https://doi.org/10.1038/s41598-017-00722-7.

Li, G., Y. K. Tan, C. Y. Li, S. C. Chen, T. Bai, D. Y. Yang, and Y. Zhang, 2015: Characteristics of boreal winter total ozone distribution in the northern hemisphere and their relationship with stratospheric temperature during recent 30 years. *Chinese Journal of Geophysics*, **58**(5), ~~1475~~213--~~1491~~228, https://doi.org/10.1002/cjg2.220168.

Lu, X., ~~L. Zhang, Y. Zhao, D. J. Jacob, Y. Hu, L. Hu, M. Gao, X. Liu, I. Petropavlovskikh, A. McClure-Begley,~~ and Coauthors~~R. Querel~~, 2019: Surface and tropospheric ozone trends in the Southern Hemisphere since 1990: Possible linkages to poleward expansion of the Hadley circulation. *Science Bulletin*, **64**, 400--409, https://doi.org/10.1016/j.scib.2018.12.021~~, 2019~~.

Marsing, A., ~~T. Jurkat-Witschas, J. U. Grooβ, S. Kaufmann, R. Heller, A. Engel, P. Hoor,~~ and Coauthors~~C. Voigt~~, 2019: Chlorine partitioning in the lowermost Arctic vortex during the cold winter 2015/2016. *Atmospheric Chemistry and Physics*, **19**(16), 10 757--10 772, https://doi.org/10.5194/acp-19-10757-2019.

Meller, R., and G. K. Moortgat, 2000: Temperature dependence of the absorption cross sections of formaldehyde between 223 and 323 K in the wavelength range 225–375 nm. *J. Geophys. Res.*, **105**(D6), 7089--7101, https://doi.org/10.1029/1999JD901074.

Nakajima, H., ~~I. Murata, Y. Nagahama, H. Akiyoshi, K. Saeki, T. Kinase, M. Takeda, Y. Tomikawa,~~ and Coauthors~~N. B. Jones~~, 2020: Chlorine partitioning near the polar vortex edge observed with ground-based FTIR and satellites at Syowa Station, Antarctica, in 2007 and 2011. *Atmospheric Chemistry and Physics*, **20**(2), 1043--1074, https://doi.org/10.5194/acp-20-1043-2020.

Nash, E. R., P. A. Newman, J. E. Rosenfield, and M. R. Schoeberl, 1996: An objective determination of the polar vortex using Ertel's potential vorticity. *J. Geophys. Res.*, **101**(D5), 9471--9478, https://doi.org/10.1029/96JD00066.

Paschou, P., M. E. Koukouli, D. Balis, C. Lerot, and M. van~~.~~ Roozendael,~~.~~ 2020: The effect of considering polar vortex dynamics in the validation of satellite total ozone observations. *Atmospheric Research*, **238**, 104870, https://doi.org/10.1016/j.atmosres.2020.104870.

Perner, D., A. Roth, and T. Klüpfel, ~~2013~~1994: Groundbased measurements of stratospheric oclo, NO_2, and O_3 at søndre strømfjord in winter 1991/92. *Geophys. Res. Lett.*, **21**(13), 1367--1370, https://~~dx.~~doi.org/10.1029/93GL01871.

Platt, U., and J. Stutz, 2008: *Differential Optical Absorption Spectroscopy: Principles and Applications*~~,~~. ~~Physics of Earth and Space Environments,~~ Springer~~-Heidelberg~~, 568 pp, https://doi.org/10.1007/978-3-540-75776-4.

Pommereau, J. P., 1982: Observation of NO_2~~NO_2~~ diurnal variation in the stratosphere. *Geophys. Res. Lett.*, **9**(8), 850--853, https://~~dx.~~doi.org/10.1029/gl009i008p00850.

Solomon, S., D. J. I~~L~~vy, D. Kinnison, M. J. Mills, R. R. Neely III, and A. Schmidt, 2016: Emergence of healing in the Antarctic ozone layer. *Science*~~.~~, **353**(6296), 269--274, https://doi.org/10.1126/science.aae0061~~https://science.sciencemag.org/content/353/6296/269~~.

Sonkaew, T., S. von~~.~~ Savigny, K. U. Eichmann, M. Weber, A. Rozanov, H. Bovensmann, and J. P. Burrows, 201~~1~~3: Chemical ozone losses in Arctic and Antarctic polar winter/spring season derived from SCIAMACHY limb measurements 2002–2009. *Atmospheric Chemistry and Physics*, **13**(4), 1809--1835, https://doi.org/10.5194/acp-13-1809-2013.

Stutz, J., and U. Platt, 1997: Improving long-path differential optical absorption spectroscopy ~~(DOAS)~~ with a quartz-fiber mode~~-~~ mixer. *Appl. Opt.*, **36**(6), 1105--1115, https://doi.org/10.1364/AO.36.001105.

Thomas, H. E., I. M. Watson, S. A. Carn~~. Simon~~, A. J. Prata, and V. J. Realmuto, 2011: A comparison of AIRS, MODIS and OMI Sulphur dioxide retrievals in volcanic clouds. *Geomatics, Natural Hazards and Risk*, **2**, 217--232, https://doi.org/10.1080/19475705.2011.564212.

Vandaele, A. C., C. Hermans, P. C. Simon, M. van~~.~~ Roozendael, J. M. Guilmot, M. Carleer, and R. Colin, 1996: Fourier transform measurement of NO_2 absorption cross-section in the visible range at room temperature. *Journal of Atmospheric Chemistry*~~*J. Atmos. Chem.*~~, **25**(3), 289--305, https://doi.org/10.1007/BF00053797.

Xie, B., H. Zhang, Z. L. Wang, S. Y. Zhao, and ~~F~~Q. ~~Qiang~~Fu, 2016: A modeling study of effective radiative forcing and climate response due to tropospheric ozone. *Adv. Atmos. Sci.*, **33**, 819--828, https://doi.org/10.1007/s00376-016-5193-0.

Zhang, Y. L., Y. Liu, C. X. Liu, and V. F. Sofieva, 2015: Satellite measurements of the madden–julian oscillation in wintertime stratospheric ozone over the Tibetan plateau and East Asia. *Adv*. *Atmos*. *Sci*., **32**(11), 1481--1492, https://doi.org/10.1007/s00376-015-5005-y.

Table 1. Fitting parameters of spectral retrieval.

O_3	223K，243K，Bogumil et al.，2003
NO_2	298K，VanDaele et al.，1996
O_4	293K，Hermans et al.，2013
Ring	Ring.exe
Fitting Interval	320nm-340nm
Polynomial	5

Table 2. The parameter nodes to estimate the AMF uncertainty on wavelength

Parameters	Nodes
SZA	35°,40°,45°, 50°, 55°, 60°, 65°, 70°, 75°,80°
Surface albedo	0.05, 0.1, 0.2, 0.3, 0.4, 0.5, 0.6
Wavelength	From 320 to 340nm in 0.5 nm interval

Table 3. The number of days inside and outside the polar vortex.

Date	2017	2018	2017.9-10	2018.9-10
Days inside polar vortex	273	235	39	45
Days outside polar vortex	92	130	22	16

Table 4. The averaged ozone VCDs and days of ozone holes.

Date	2017	2017.9-10	2018	2018.9-10	2019	2019.9-10
Average ozone VCDs (DU)	295.85	260.76	289.32	215.13	294.04	283.38
Days of ozone holes	16	15	30	25	29	22

Fig. 1. The location and instrument of our experiment. The red star denotes the location of our experimental site. The red and yellow regions denote the pixels of OMI and GOME-2 observations.

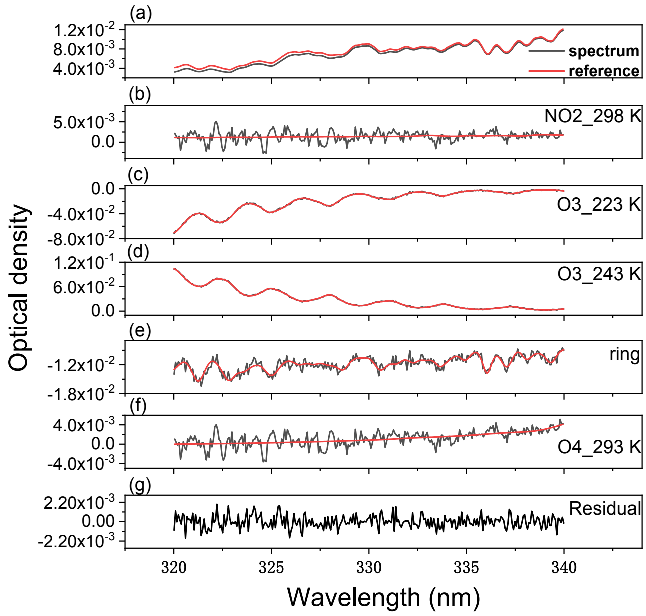

Fig. 2. The spectrum fits of ozone on February 24, 2018.

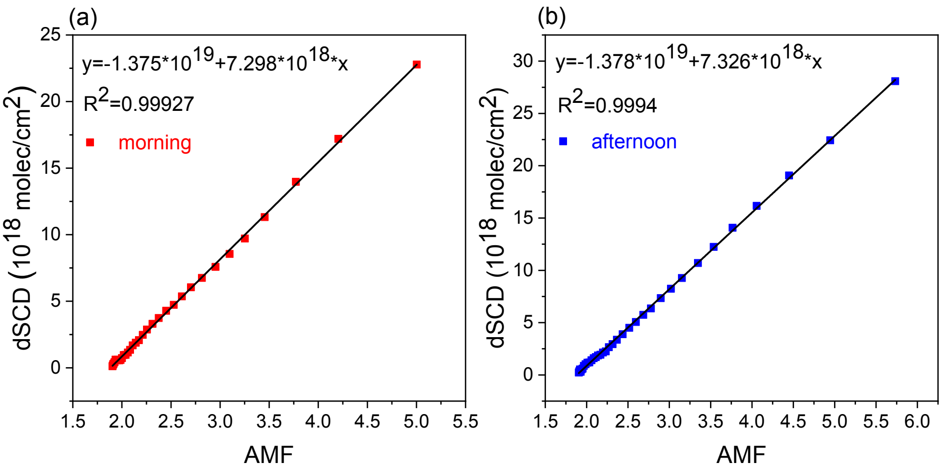

Fig. 3. Linear fitting between ozone dSCDs and AMFs on morning (a) and afternoon (b) of February 24, 2018. The correlation coefficients (R^2) are 0.99927 and 0.9994. The ozone VCDs of morning and afternoon are $7.298 \times 10^{18}\,\mathrm{molec/cm^2}$ and $7.326 \times 10^{18}\,\mathrm{molec/cm^2}$. The calculated ozone VCD of February 24, 2018 is $7.322 \times 10^{18}\,\mathrm{molec/cm^2}$.

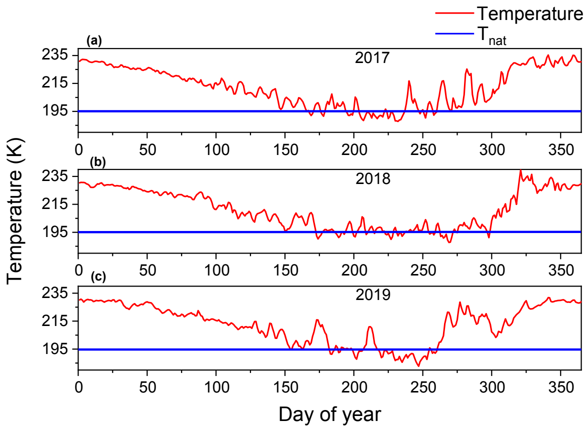

Fig. 4. The temperatures (at 50 hPa) over Fildes Peninsula from 2017 to 2019, where the blue lines denote the threshold temperature for the formation of PSCs.

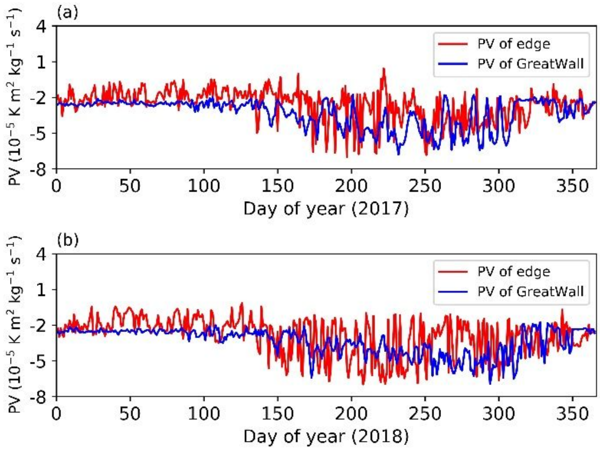

Fig. 5. The PV (on isentropic level of 475 K) of the Fildes Peninsula and vortex edge, where red and blue lines denote PV of vortex edge (calculated by Nash's criterion) and Fildes Peninsula respectively. (a) The PV in 2017. (b) The PV in 2018.

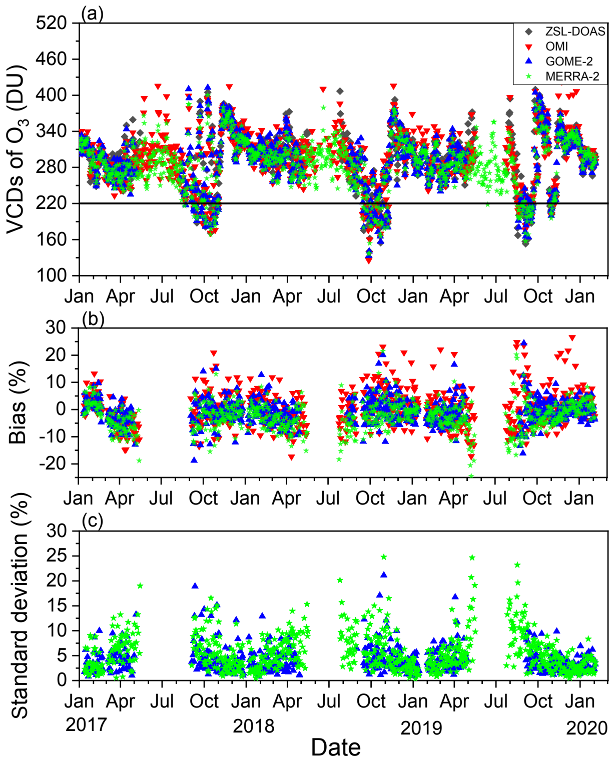

Fig. 6. (a) The ozone VCDs of ZSL-DOAS, OMI, GOME-2, and MERRA-2. The black line denotes the threshold for ozone holes. (b) The biases of OMI, GOME-2 and MERRA-2. (c) The standard deviations of GOME-2 and MERRA-2.

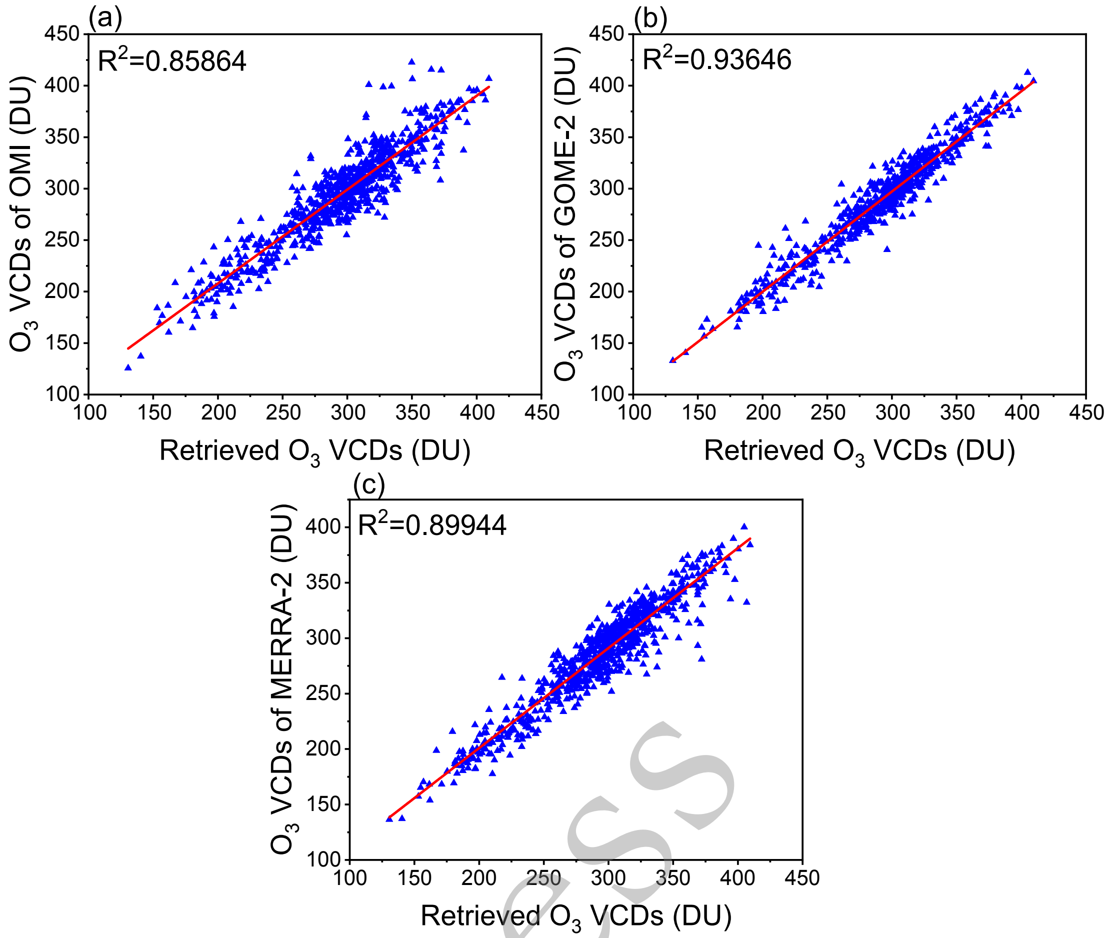

Fig. 7. (a) The scatter plots and linear fit of retrieved ozone VCDs with OMI. (b) The scatter plots and linear fit of retrieved ozone VCDs with GOME-2. (c) The scatter plots and linear fit of retrieved ozone VCDs with MERRA-2.

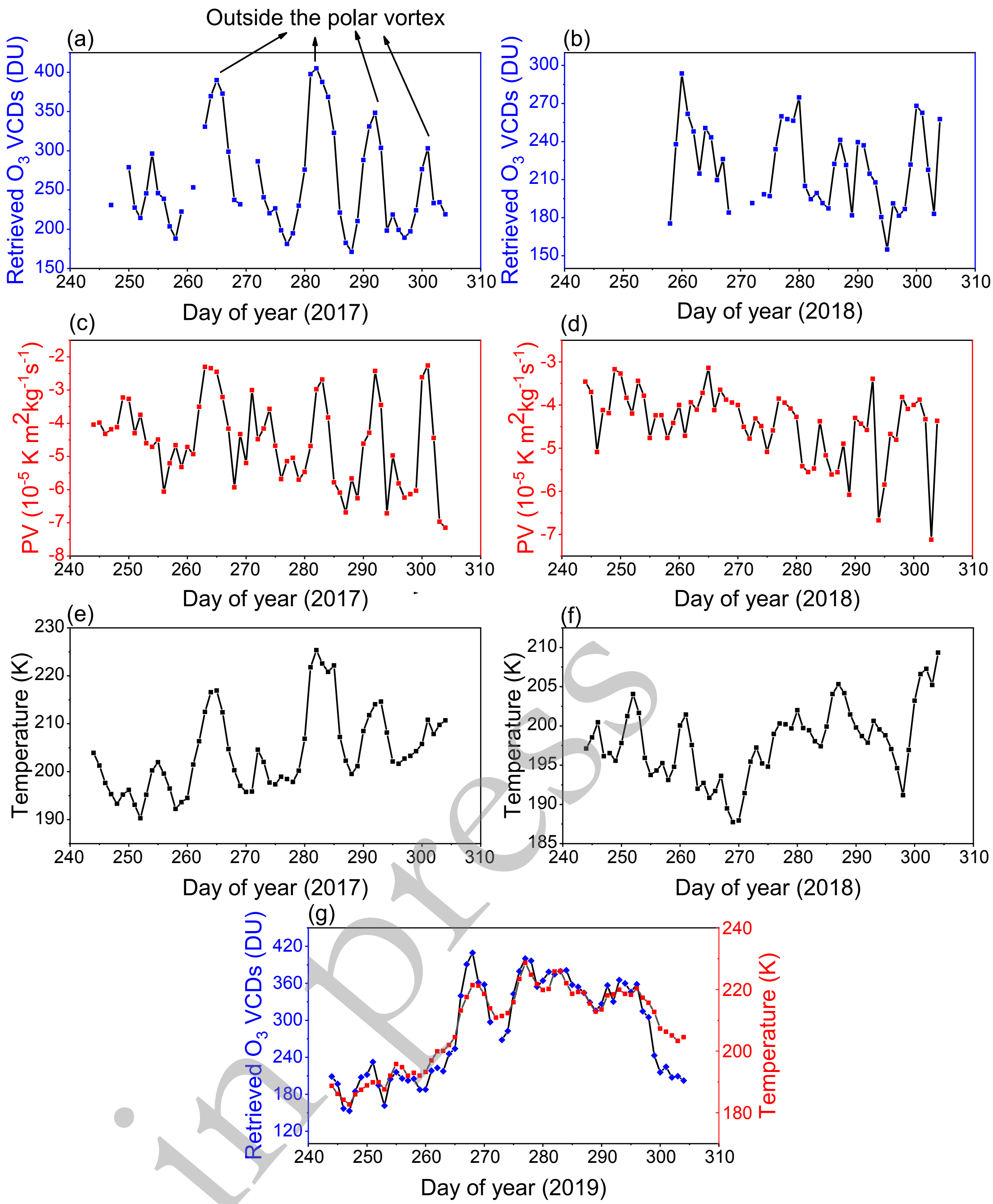

Fig. 8. The ozone VCDs, PV and temperatures (at 50 hPa) from September to October during the observation periods: (a) the retrieved ozone VCDs from September to October in 2017; (b) the retrieved ozone VCDs from September to October in 2018; (c) the PV (at 50 hPa) from September to October in 2017; (d) the PV (at 50 hPa) from September to October in 2018; (e) the temperature (at 50 hPa) from September

to October in 2017; (f) the temperature (at 50 hPa) from September to October in 2018; (g) the retrieved ozone VCDs and temperature (at 50 hPa) from September to October in 2019.

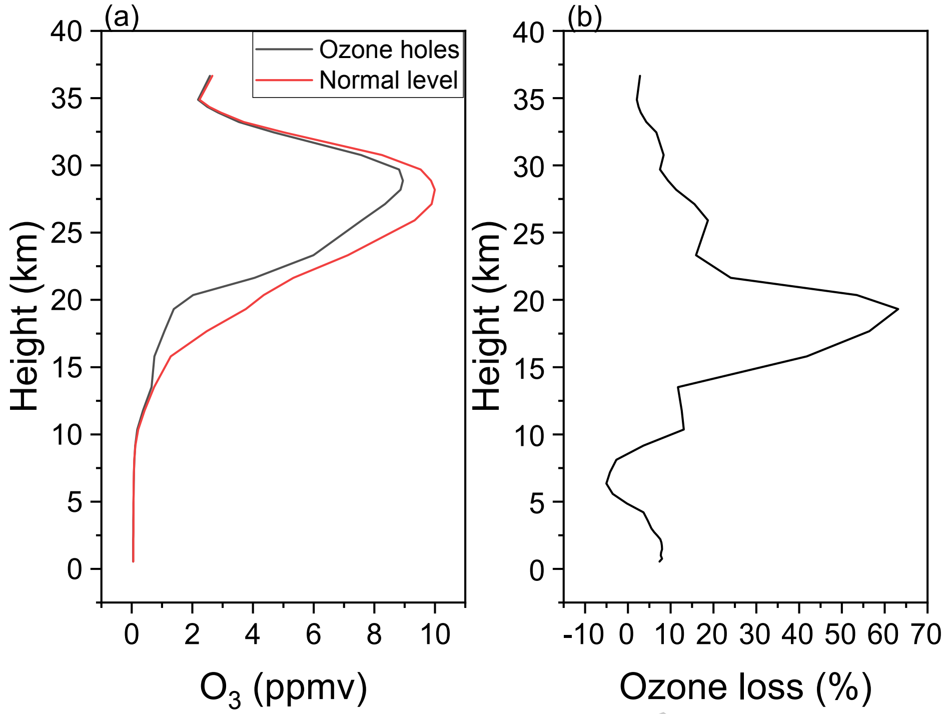

Fig. 9. (a) The averaged ozone profiles during the ozone hole periods and non-ozone hole periods from September to October in 2017. (b) The percentage of ozone loss at different heights calculated by (a).

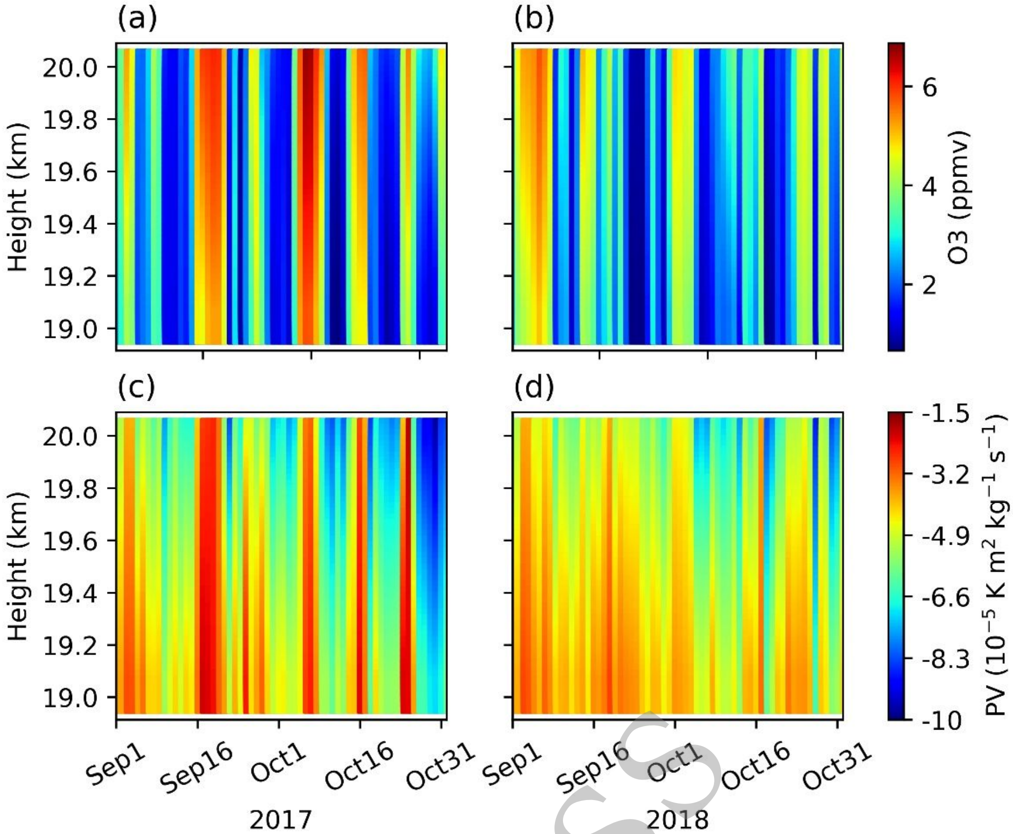

Fig. 10. The profiles of ozone and PV from September to October in 2017 and 2018, at the height of 19-20 km: (a) the profile of ozone in 2017; (b) the profile of ozone in 2018; (c) the profile of PV in 2017; (d) the profile of PV in 2018.